

## Asymmetric coupling in two-lane simple exclusion processes with Langmuir kinetics: Phase diagrams and boundary layers

Arvind Kumar Gupta\* and Isha Dhiman

*Department of Mathematics, Indian Institute of Technology Ropar, Rupnagar-140001, India*

(Received 18 September 2013; revised manuscript received 4 December 2013; published 21 February 2014)

We use boundary layer analysis for an open system consisting of two parallel totally asymmetric simple exclusion processes with Langmuir kinetics under a biased lane-changing rule. The two kinds of phase transitions—bulk transitions and surface transitions—have been examined. The dynamics of shock and their dependence on the system parameters have been investigated. We find a reduction in the number of steady-state phases with increase in lane-changing rate.

DOI: [10.1103/PhysRevE.89.022131](https://doi.org/10.1103/PhysRevE.89.022131)

PACS number(s): 02.50.Ey, 64.60.-i, 05.70.Ln, 05.60.-k

The asymmetric simple exclusion process (ASEP) is the simplest model for studying driven diffusive systems, in which particles hop in a preferred direction along the lattice. Despite their simplicity, ASEPs can explain some complex nonequilibrium phenomena such as boundary-induced phase transitions [1], phase separation [2], symmetry breaking [3], and shock formation [4–6].

In a totally asymmetric simple exclusion process (TASEP) connected to boundary reservoirs, the total number of particles remains conserved in the bulk. Recently, a lot of attention has been given to the exclusion processes coupled with a bulk reservoir, where the particles can attach and/or detach at bulk sites [Langmuir kinetics (LK)]. The LK dynamics violate particle conservation in the bulk. Single-channel TASEP coupled with LK has been studied comprehensively [7,8]. The competing dynamics of particle conservation (TASEP) and particle nonconservation (LK) in a single-channel lattice results in the localization of shocks. This is in contrast to the TASEP without LK, where shocks move with a constant velocity and are driven out of the system. A few studies have been reported in the literature which investigate multichannel TASEP models with LK [9]. The steady-state dynamics of two-channel symmetrically coupled TASEP with LK are the same as that of the corresponding single-channel model because of the symmetry in lane-changing rates.

The present work explores the consequences of asymmetric coupling conditions in a two-lane totally asymmetric simple exclusion process with Langmuir kinetics. We consider a two-lane open system consisting of two parallel one-dimensional lattice channels, A and B, each with  $L$  sites. The state of the system is defined by a set of occupation numbers  $n_j^i$  ( $i = 1, 2, 3, \dots, L$ ;  $j = A, B$ ), each of which is either zero (vacant site) or one (occupied site). The system consists of indistinguishable particles distributed under the hard-core exclusion principle. For each time step, a lattice site  $(i, j)$  is randomly chosen. At entrance ( $i = 1$ ), a particle can enter the lattice with rate  $\alpha$  when  $n_j^1 = 0$ ; and at exit ( $i = L$ ), a particle can leave the lattice with rate  $\beta$  when  $n_j^L = 1$ . If  $n_A^i = 1$  ( $i = 2, 3, \dots, L - 1$ ), then the particle will first try to detach itself from the site with a rate  $w_d$ . If it cannot detach from site  $(i, A)$ , it will jump to site  $(i + 1, A)$  with unit rate

provided  $n_A^{i+1} = 0$ ; otherwise it shifts to lane B with rate  $w$  if  $n_B^i = 0$ . If  $n_A^i = 0$ , then a particle attaches to the site with a rate  $w_a$ . The dynamics in lane B are similar, with the only exception being that particles are forbidden to shift from lane B to lane A.

The temporal evolution of bulk particle densities ( $1 < i < L$ ) in the two lanes is given by the master equation

$$\begin{aligned} \frac{d\langle n_{A,B}^i \rangle}{dt} = & \langle n_{A,B}^{i-1} (1 - n_{A,B}^i) \rangle - \langle n_{A,B}^i (1 - n_{A,B}^{i+1}) \rangle \\ & + \omega_a \langle 1 - n_{A,B}^i \rangle - \omega_d \langle n_{A,B}^i \rangle \mp \omega \langle n_A^i n_A^{i+1} (1 - n_B^i) \rangle, \end{aligned}$$

where  $\langle \dots \rangle$  denotes the statistical average. The last term takes a negative sign for lane A and positive for lane B. At boundaries, the particle densities evolve as

$$\frac{d\langle n_j^1 \rangle}{dt} = \alpha \langle (1 - n_j^1) \rangle - \langle n_j^1 (1 - n_j^2) \rangle, \quad (1)$$

$$\frac{d\langle n_j^L \rangle}{dt} = \langle n_j^{L-1} (1 - n_j^L) \rangle - \beta \langle n_j^L \rangle. \quad (2)$$

The continuum limit of the model in a mean-field approximation can be obtained by coarse-graining a discrete lattice with lattice constant  $\epsilon = 1/L$  and rescaling the time as  $t' = t/L$ . Define  $\Omega_a = \omega_a L$ ,  $\Omega_d = \omega_d L$ , and  $\Omega = \omega L$ . Rewriting  $\langle n_j^i \rangle = \rho_j^i$  and dropping the superscript  $i$ , since both lattices are free of any kind of spatial inhomogeneity, we get

$$\begin{aligned} \frac{\partial}{\partial t'} \begin{bmatrix} \rho_A \\ \rho_B \end{bmatrix} + \frac{\partial}{\partial x} \begin{bmatrix} -\frac{\epsilon}{2} \frac{\partial \rho_A}{\partial x} + \rho_A (1 - \rho_A) \\ -\frac{\epsilon}{2} \frac{\partial \rho_B}{\partial x} + \rho_B (1 - \rho_B) \end{bmatrix} \\ = \begin{bmatrix} \Omega_a (1 - \rho_A) - \Omega_d \rho_A - \Omega \rho_A^2 (1 - \rho_B) \\ \Omega_a (1 - \rho_B) - \Omega_d \rho_B + \Omega \rho_A^2 (1 - \rho_B) \end{bmatrix}, \quad (3) \end{aligned}$$

where  $\rho_{A,B}$  is the average density in lanes A and B. The right-hand side represents the nonconservative terms formed by combination of lane-changing transitions and Langmuir kinetics. Under the case  $\Omega_a = \Omega_d$ , system (3) in the steady state reduces to

$$\frac{\epsilon}{2} \frac{d^2 \rho_{A,B}}{dx^2} + (2\rho_{A,B} - 1) \left( \frac{d\rho_{A,B}}{dx} - \Omega_d \right) \mp \Omega \rho_A^2 (1 - \rho_B) = 0, \quad (4)$$

\*akgupta@iitrpr.ac.in

with the boundary conditions  $\rho_A(0) = \rho_B(0) = \alpha$ ,  $\rho_A(1) = \rho_B(1) = 1 - \beta = \gamma$  (say).

The coupling term  $\Omega\rho_A^2(1 - \rho_B)$  acts as a sink for lane A and source for lane B and its presence restrains us from finding the explicit solutions for average densities in both lanes. We use a combination of boundary layer analysis and numerical techniques to obtain bulk (outer) and boundary layer (inner) solutions separately and then match these solutions suitably. The outer solution is found in the limit  $\epsilon \rightarrow 0$ . This gives an over-determined system of first-order equations, which cannot fulfill the four boundary conditions simultaneously. The density profiles in the steady state have been obtained numerically [9] by keeping the time derivative terms in the system and capturing the solution after sufficiently long time to ensure the occurrence of a steady state. For the inner solution, we define  $\tilde{x} = \frac{x-x_d}{\epsilon}$ , where  $x_d$  is the position of the boundary layer. This rescaling leads to elimination of the source and sink terms in the system of hydrodynamic equations, which is well justified because particle-nonconserving dynamics are irrelevant in regions of width of  $O(\epsilon)$ . In terms of  $\tilde{x}$ , the inner solution  $\rho_{j,\text{in}}$  is given by

$$\frac{d\rho_{j,\text{in}}}{d\tilde{x}} = 2(a_j + \rho_{j,\text{in}} - \rho_{j,\text{in}}^2). \quad (5)$$

Here, the integration constant  $a_j$  is computed from the matching condition of outer and inner solutions. Suppose the boundary layer appears at the right boundary ( $x = 1$ ) in lane  $j$ , the matching condition requires  $\rho_{j,\text{in}}(\tilde{x} \rightarrow -\infty) = \rho_{j,\text{out}}(x = 1) = \rho_{j,o}$  (say). Here,  $\rho_{j,o}$  is the value of the left outer solution in lane  $j$  at  $x = 1$ . Clearly,  $\rho_{j,o}$  is a function of system parameters  $\Omega_d$  and  $\Omega$ . The lane-changing and attachment-detachment phenomena impart their effects in the inner solution through the matching conditions. Solving Eq. (5) with  $a_j = \rho_{j,o}^2 - \rho_{j,o}$ , we get  $\rho_{j,\text{in}} = \frac{1}{2} + \frac{|2\rho_{j,o}-1|}{2} \tanh(\frac{\tilde{x}}{w_j} + \xi_j)$ , where  $w_j = \frac{1}{|2\rho_{j,o}-1|}$  and  $\xi_j = \tanh^{-1}(\frac{2\rho_{j,o}-1}{|2\rho_{j,o}-1|})$ . Being computed from the left boundary condition,  $\rho_{j,o}$  is a function of  $\alpha$ , so  $\xi_j$  becomes a function of  $\alpha$  as well as  $\gamma$ . This gives a density profile with the right boundary layer (rbl) in lane  $j$  with a positive slope ( $\tanh -r$ ), which exists for  $\gamma > \rho_{j,o}(\alpha)$ . As  $\tilde{x} \rightarrow \infty$ , the boundary layer at  $x = 1$  saturates to  $\rho_{j,s}$  (say) given by  $\rho_{j,o}^2 - \rho_{j,o} + \rho_{j,s} - \rho_{j,s}^2 = 0$ , equivalent to  $\rho_{j,s} = 1 - \rho_{j,o}$ . When  $\gamma > \rho_{j,s}(\alpha)$ , the inner solution fails to satisfy the right boundary condition  $\rho_{j,\text{in}}(\tilde{x} \rightarrow \infty) = \gamma$  and deconfines from the boundary to enter the bulk of lane  $j$  in the form of a shock. Thus  $\gamma = 1 - \rho_{j,o}(\alpha)$  acts as a bulk transition line between low-density (LD) and shock (S) phases. Such a continuous transition is reminiscent of the bulk transition observed in single-channel TASEP with LK [8], known as a shockening transition. Within the LD phase, the slope of the boundary layer is negative for  $\gamma < \rho_{j,o}(\alpha)$  and the inner solution in this region is  $\rho_{j,\text{in}} = \frac{1}{2} + \frac{|2\rho_{j,o}-1|}{2} \coth(\frac{\tilde{x}}{w_j} + \hat{\xi}_j)$ , where  $\hat{\xi}_j = \coth^{-1}(\frac{2\rho_{j,o}-1}{|2\rho_{j,o}-1|})$ . Here, the change in the slope of the boundary layer describes a surface transition. The length scale described by  $\hat{\xi}_j$  shows a logarithmic divergence ( $\hat{\xi}_j \sim \ln|\gamma - \rho_{j,o}|$ ) as one approaches the surface transition line from either direction in the phase plane. On the surface transition curve, i.e.,  $\rho_{j,o} = \gamma$ , we get a density profile without a boundary layer. Fixing  $\alpha$ , if one reduces the withdrawal

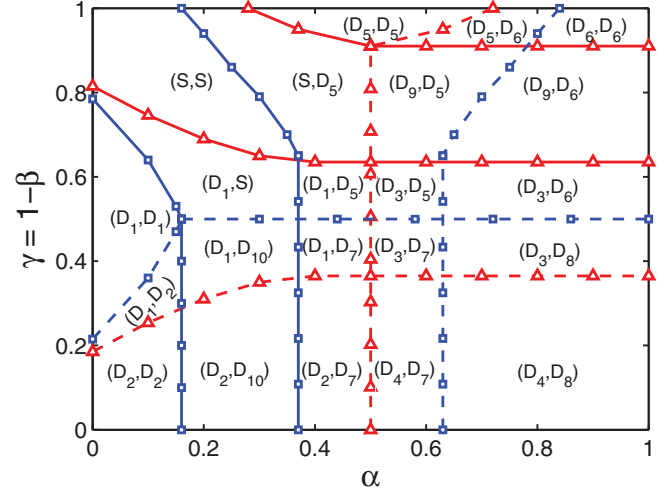


FIG. 1. (Color online) Phase diagram for  $\Omega_d = 0.2$  and  $\Omega = 1$ .  $D_1$ :  $\tanh-r$ ,  $D_2$ :  $\coth-r$ ,  $D_3$ :  $\tanh-r$  with lbl,  $D_4$ :  $\coth-r$  with lbl,  $D_5$ :  $\tanh-l$ ,  $D_6$ :  $\coth-l$ ,  $D_7$ :  $\tanh-l$  with rbl,  $D_8$ :  $\coth-l$  with rbl,  $D_9$ : S+lbl and  $D_{10}$ : S + rbl. Curves marked with triangles and squares represent phase boundaries of lanes A and B, respectively. Solid (dashed) curves denote bulk (surface) transitions.

rate of particles, particles start accumulating near the right boundary forming an increasing boundary layer. Similarly, reducing  $\gamma$  increases the withdrawal rate which creates a scarcity of particles near the right boundary and justifies the formation of a decaying right boundary layer. Along similar lines, one can analyze the boundary layer at  $x = 0$ .

We have obtained the phase diagram for  $\Omega_d = 0.2$  and  $\Omega = 1$ . The biased lane-changing rule generates a richer and more complex phase diagram (Fig. 1). To gain deeper insight into the various phase transitions, we inspect the topology of the phases for each lane separately (Fig. 2). The LD phase in  $\alpha$ - $\gamma$  phase plane for lane A comprises of two major parts ( $\alpha < 1/2$  and  $\alpha > 1/2$ ), each of which is further divided into two subregions by a surface transition line  $L_1$ . When  $\alpha > 1/2$ , the bulk density (less than  $1/2$ ) is not compatible with the boundary condition  $\rho_A(x = 0) = \alpha$ , which produces a decaying boundary layer at  $x = 0$ . Across the curve  $L_2$ , one finds the formation of shock through the shockening transition, while the dynamics at the left boundary remain preserved. In the S phase, the density profile comprises a shock with a left boundary layer (lbl) for  $\alpha > 1/2$ . Further,

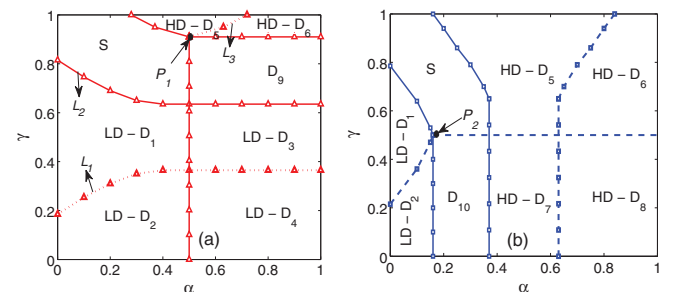


FIG. 2. (Color online) Phase diagrams for (a) lane A and (b) lane B. The notation and parameters are the same as in Fig. 1.

an increase in  $\gamma$  leads to a leftward motion of shock in the bulk, until it reaches  $x = 0$  to produce a high-density (HD) profile with a tanh-type left boundary layer (tanh-l). The HD phase also involves surface transition  $L_3$ , which leads to formation of two subregions, viz.,  $1 - \rho_{A,o}(\gamma) < \alpha < \rho_{A,o}(\gamma)$  and  $\alpha > \rho_{A,o}(\gamma)$ . Here,  $\rho_{A,o}(\gamma)$  is the value of the right outer solution at  $x = 0$ . The intersection of lines  $\alpha = \rho_{A,o}(\gamma)$  and  $\alpha = 1 - \rho_{A,o}(\gamma)$  locates a critical point ( $\alpha_{cA}, \gamma_{cA}$ ) in the phase plane (marked  $P_1$ ), where  $\alpha_{cA} = 1/2$  and  $\gamma_{cA}$  is given by  $\rho_{A,o}(\gamma_{cA}) = 1/2$ . Across the phase boundary between the S and HD phases, i.e.,  $\alpha = 1 - \rho_{A,o}(\gamma)$  and  $\alpha < \alpha_{cA}$ , shock is formed due to deconfinement of the tanh-l type inner solution, while the coth-l boundary layer in  $\alpha > \rho_{A,o}(\gamma)$  does not deconfine to produce shock. Here,  $\gamma_{cA}$  remains the critical value of  $\gamma$  for  $\alpha > \alpha_{cA}$ , which gives the horizontal transition line  $\gamma = \gamma_{cA}$  as the phase boundary between the HD and S phases. The various phase boundaries and critical point  $P_2$  for lane B can also be obtained similarly as discussed for lane A.

Lane A can be thought of as a homogeneous bulk reservoir of particles for lane B. So, in addition to attachment and detachment occurring due to LK, more particles detach from lane A and attach to lane B. This creates an imbalance between attachment and detachment rates in both lanes. Now, the effective detachment rate in lane A (B) has become higher (lower) than the effective attachment rate in lane A (B). Due to this reason, the structure of the phase diagram for lane A and lane B comes out qualitatively similar to that of a single-channel TASEP with LK for  $\Omega_a < \Omega_d$  (more detachment) and  $\Omega_a > \Omega_d$  (more attachment), respectively [8].

Figure 3(a) shows six distinct steady-state phases, viz., (LD, LD), (LD, S), (S, HD), (S, S), (HD, HD), and (LD, HD) for  $\Omega_d = 0.2$  and  $\Omega = 1$ . On comparing Fig. 3(a) with the phase diagram of an uncoupled system for  $\Omega_a = \Omega_d$  [8], one finds that a major part of the phase plane is covered by the (LD, HD) phase due to the absence of a maximal-current (MC) phase in our system. Also, the region of the LD (HD) phase expands while that of the HD (LD) phase shrinks in lane A (B). This is physically justified because the shifting

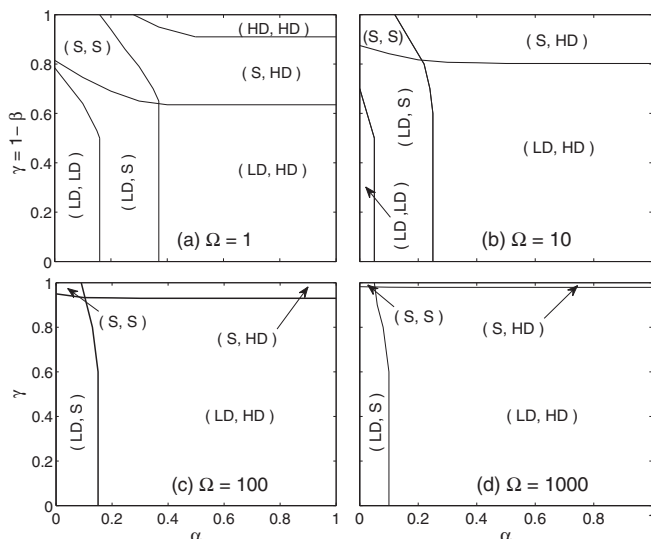


FIG. 3. Effect of  $\Omega$  on the phase diagram for  $\Omega_d = 0.2$ .

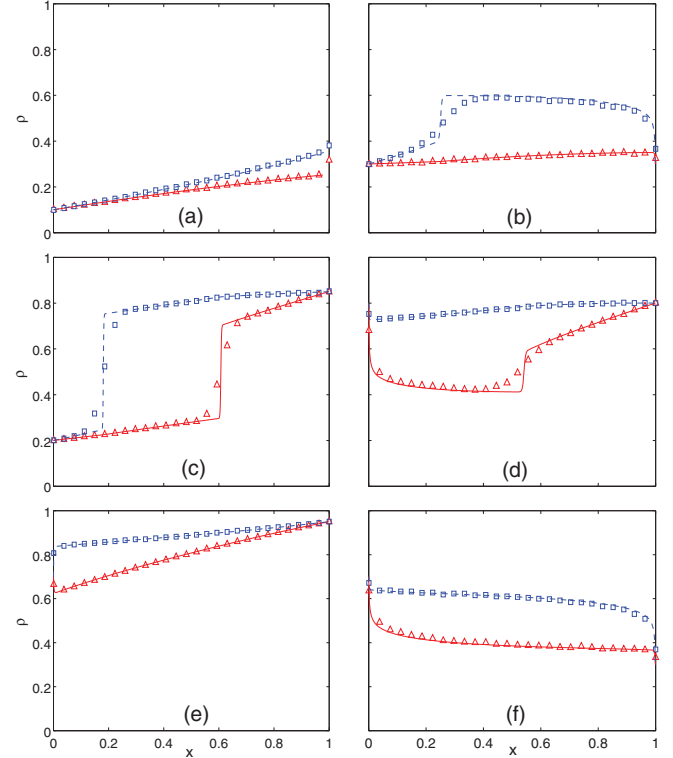


FIG. 4. (Color online) Density profiles with  $\Omega_d = 0.2$ ,  $\Omega = 1$ . The continuum mean-field density profiles are shown by red (blue) and solid (dashed) in lane A (B). The curves marked with triangles (squares) show Monte Carlo simulation results for lane A (B). (a) (LD, LD) phase for  $\alpha = 0.1, \gamma = 0.4$ ; (b) (LD, S) for  $\alpha = 0.3, \gamma = 0.3$ ; (c) (S, S) phase for  $\alpha = 0.2, \gamma = 0.85$ ; (d) (S, HD) phase for  $\alpha = 0.8, \gamma = 0.8$ ; (e) (HD, HD) phase for  $\alpha = 0.7, \gamma = 0.95$ ; and (f) (LD, HD) phase for  $\alpha = 0.7, \gamma = 0.3$ .

of additional particles from lane A to B creates a relative shortage (abundance) of particles in lane A (B). Therefore,  $\rho_A < \rho_B$  by virtue of which we have nonexistence of (S, LD), (HD, S), and (HD, LD) steady-state phases. Figure 3(b) shows the steady-state phase diagram with  $\Omega = 10$ , which indicates an enlargement (shrinkage) in the region confined to the LD (HD) phase. The reverse phenomenon happens for phases in lane B. This combined effect can be seen from the phase diagram, where the major part of the phase plane is covered by the (LD, HD) phase. Note that the number of steady-state phases is reduced to five due to the disappearance of the (HD, HD) phase. For  $\Omega = 100$ , the number of steady-state phases further reduces to four with the exclusion of (LD, LD) phase [Fig. 3(c)]. For  $\Omega = 1000$ , the (S, S), (LD, S), and (S, HD) phases are confined to a very small region [Fig. 3(d)]. Figure 4 shows the density profiles from continuum mean-field equations and their validation using Monte Carlo simulations obtained for  $L = 1000$ . Since the size of a real system is normally not very large, it is reasonable to simulate the system for a lattice size up to 1000 to realistically describe the motion of motor proteins [9]. The Monte Carlo simulations are carried out for  $10^{10}$ – $10^{11}$  time steps and the first 5% steps are ignored to ensure the occurrence of a steady state. The densities in both

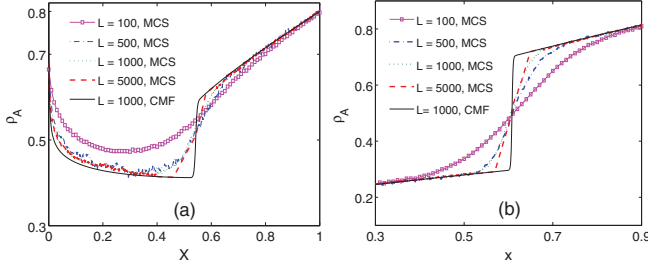


FIG. 5. (Color online) (a) Width of the transition region formed by the left boundary layer in lane A decreases with increase in system size for  $\alpha = 0.8, \gamma = 0.8$ . (b) Effect of system size on shock profile in lane A for  $\alpha = 0.2, \gamma = 0.85$  with Monte Carlo simulation (MCS). The steepness of the shock increases with increase in system size. The dashed profiles are the continuum mean-field (CMF) result for  $L = 1000$ .

the lanes have been computed by taking time averages over an interval of  $10L$ .

We have investigated the effect of lattice size on the density profiles and observed that the bulk solution given by Monte Carlo simulations is independent of lattice size. However, it is found that the width of the transition region of boundary layer decreases as the number of lattice sites increases [Fig. 5(a)]. This indicates that the boundary layer is a finite-size effect which disappears in the limit of an infinite system. Similarly, one finds an increase in the sharpness in the steep rise of the shock with an increase in system size [Fig. 5(b)]. For the sake of clarity, average densities in only one of the two lanes, viz., lane A, are shown in Fig. 5. These observations are consistent with the results reported in the literature [9].

A discontinuity in the bulk connecting a low (high)-density part on the left to a high (low)-density part on the right is known as upward (downward) shock. An interesting observation is that no downward shock is possible in our system. The nonexistence of downward shock in lane B would imply the same for lane A and vice versa. Figure 6(a) and the inset show the situations when density in either lane incurs a downward shock. Both situations violate  $\rho_A < \rho_B$ . Therefore, it is sufficient to show that there does not exist a downward shock in lane B. This is justified with the help of fixed-point theory [10]. Ignoring the contribution of particle-nonconserving terms in the boundary layer or shock regions, we set these terms to zero in the system (4) to get  $\rho_A = f(\rho_B)$  (say). System (4) gives

$$\frac{\epsilon}{2} \left( \frac{d\rho_A}{dx} + \frac{d\rho_B}{dx} \right) + \rho_A^2 - \rho_A + \rho_B^2 - \rho_B = c. \quad (6)$$

Here,  $c$  is a constant of integration. The fixed points of Eq. (6) are given by  $\rho_A^2 - \rho_A + \rho_B^2 - \rho_B = c$ . Substituting  $\rho_A = f(\rho_B)$ , we obtain a two-dimensional fixed-point diagram in the  $c$ - $\rho_B$  plane [Fig. 6(b)], in which the lower branch (ab) is unstable while the upper branch (bc) is stable. A downward shock is possible if a point on the curve in the upper branch can be connected to a point in the lower branch by a vertical line [10]. One can easily see from the direction of the vertical arrows that it is not possible to get a downward shock in lane B. So, we cannot get downward shock in the bulk of the

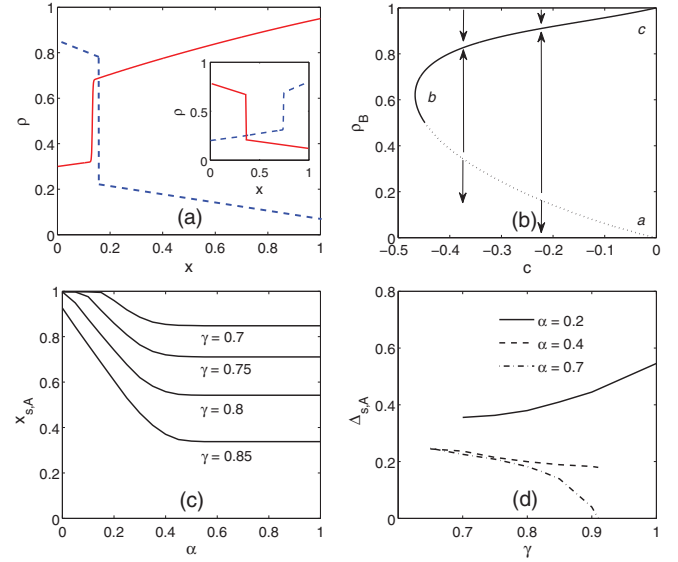


FIG. 6. (Color online) (a) Downward shock in lane B; the inset shows downward shock in lane A; (b) fixed-point diagram; (c) DW location for different values of  $\gamma$ ; and (d) height of DW for different values  $\alpha$ .

density profiles in any of the two lanes. This important result supports our previous observation that a decaying boundary layer at either boundary cannot produce a shock through its deconfinement.

We compute the position of the domain wall (DW) in lane  $j$  ( $x_{s,j}$ ) using the constancy of current across the shock, viz.,  $\rho_{j,+}^2 - \rho_{j,+} = \rho_{j,-}^2 - \rho_{j,-}$ , where  $\rho_{j,-} = \lim_{x \rightarrow x_{s,j}^-} \rho_j(x)$  and  $\rho_{j,+} = \lim_{x \rightarrow x_{s,j}^+} \rho_j(x)$ . Figure 6(c) shows that upon increasing  $\alpha$ , there is a continuous (linear) change in the position of DW from right to left in the bulk till  $\alpha \leq 1/2$  for different values of  $\gamma$  in lane A. A further increase in  $\alpha$  leads to a gradual settlement of the DW to a fixed position. This is due to the presence of a boundary layer at the entrance which obstructs the incoming particles from entering the bulk and localizes the DW. Figure 6(d) shows the variation of height of DW in lane A ( $\Delta_{s,A} = \rho_{A,+} - \rho_{A,-} = 2\rho_{A,+} - 1$ ) with respect to  $\gamma$  along lines of constant entrance rate  $\alpha$ . For  $1 - \rho_{A,o}(\gamma) < \alpha < 1/2$ ,  $\Delta_{s,A}$  jumps discontinuously to a finite value on entering the S region from the HD phase, whereas there is a continuous rise in the height from zero for  $\alpha \geq 1/2$ . Further, at the phase boundary between the LD and S phases [ $\gamma = 1 - \rho_{A,o}(\alpha)$ ],  $\Delta_{s,A}$  jumps to zero discontinuously.

In this study, we have investigated a two-lane totally asymmetric simple exclusion process with Langmuir kinetics in asymmetric coupling conditions using boundary layer analysis of continuum mean-field equations for  $\omega_a = \omega_d$ . The structure of the phase diagram of a two-lane TASEP with LK in asymmetric coupling conditions is quite complex as compared to that in symmetric coupling. The bulk transition from LD (HD) to the shock phase occurs through deconfinement of the right (left) boundary layer, and the surface transition occurs in both LD and HD phases, which changes the sign of slope of the boundary layer. We find a reduction in the number of steady-state phases in the system with increasing

lane-changing rate. We have examined the finite-size effect and found that the width of the transition region of the boundary layer reduces with an increase in system size. Fixed-point theory shows the nonexistence of a downward shock in the system. We have also analyzed the dependence of shock

on boundary rates, its motion in the bulk, position, and height.

The second author acknowledges CSIR, New Delhi, India, for providing financial support.

- 
- [1] J. Krug, *Phys. Rev. Lett.* **67**, 1882 (1991); V. Popkov, *J. Stat. Mech.* (2007) P07003; A. K. Gupta and I. Dhiman, *Physica A* **392**, 6314 (2013).
- [2] J. Krug, *Braz. J. Phys.* **30**, 97 (2000).
- [3] M. Clincy, M. Evans, and D. Mukamel, *J. Phys. A: Math. Gen.* **34**, 9923 (2001).
- [4] M. R. Evans, R. Juhasz, and L. Santen, *Phys. Rev. E* **68**, 026117 (2003).
- [5] V. Popkov, A. Rákos, R. D. Willmann, A. B. Kolomeisky, and G. M. Schütz, *Phys. Rev. E* **67**, 066117 (2003).
- [6] R. Jiang, M.-B. Hu, Y.-H. Wu, and Q.-S. Wu, *Phys. Rev. E* **77**, 041128 (2008).
- [7] A. Parmeggiani, T. Franosch, and E. Frey, *Phys. Rev. Lett.* **90**, 086601 (2003); *Phys. Rev. E* **70**, 046101 (2004).
- [8] S. Mukherji and V. Mishra, *Phys. Rev. E* **74**, 011116 (2006).
- [9] R. Jiang, R. Wang, and Q.-S. Wu, *Physica A* **375**, 247 (2007); R. Wang, R. Jiang, M. Liu, J. Liu, and Q.-S. Wu, *Int. J. Mod. Phys. C* **18**, 1483 (2007).
- [10] S. Mukherji, *Phys. Rev. E* **79**, 041140 (2009); V. Yadav, R. Singh, and S. Mukherji, *J. Stat. Mech.* (2012) P04004.